CIVIL ENGINEERING

Dam overtopping risk using probabilistic concepts – Case study: The Meijaran Dam, Iran

Ehsan Goodarzi [a,*], Lee Teang Shui [b,1], Mina Ziaei [a,2]

[a] *Dept. of Water Resources Engineering, Faculty of Engineering, University Putra Malaysia, 251 10Th St. NW, APT A608, PO 30318-5600, Atlanta, GA, USA*
[b] *Dept. of Biological and Agricultural Engineering, Faculty of Engineering, University Putra Malaysia, 3rd Floor, Engineering Faculty, UPM, Serdang 43400, Selangor*

Abstract Hydrologic risk assessment and uncertainty analysis by mathematical and statistical methods provide useful information for decision makers. This study presents the application of risk and uncertainty analysis to dam overtopping due to various inflows and wind speeds for the Meijaran Dam in the north of Iran. The procedure includes univariate flood and wind speed frequency analyses, reservoir routing, and integration of wind set-up and run-up to calculate the reservoir water elevation. Afterwards, the probability of overtopping was assessed by applying two uncertainty analysis methods (Monte Carlo simulation and Latin hypercube sampling), and considering the quantile of flood peak discharge, initial depth of water in the reservoir, and spillway discharge coefficient as uncertain variables. The results revealed that rising water level in the reservoir is the most important factor in overtopping risk analysis and that wind speed also has a considerable impact on reservoirs that are placed in windy areas.

1. Introduction

The proper design of a dam's spillway and the flood control capacity of a reservoir can ensure the safety of the dam and avoid any undesirable problems, such as overtopping. Hence, an exact estimate of flood design and extreme inflow hydrographs is required for the design of such important hydraulic structures. The flood design can be defined as the maximum flood that a structure can safely pass while the most common method for evaluating this flood is using univariate frequency analysis of recorded peak discharges. Although univariate flood frequency analysis is used to estimate peak discharges for a particular return period, dams still suffer from
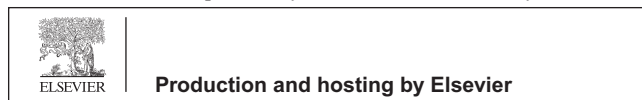
* Corresponding author. Tel.: +1 404 944 6539.
E-mail addresses: ehsan.goodarzi@gatech.edu, Ehsan.g@hotmail.com (E. Goodarzi), tslee@eng.upm.edu.my (L. Teang Shui), mina.ziaei@gatech.edu (M. Ziaei).
[1] Tel.: +6 012 629 9749.
[2] Tel.: +1 404 944 7431.

Nomenclature

C	spillway discharge coefficient	Q	outflow (cms)
D	mean water depth along the fetch length (m)	R	resistance
F	fetch length (km)	S	storage (MCM)
F_x^{-1}	inverse function	t	time (s)
H_0	average depth of water from bed (m)	T	flood return period
H	wave height (m)	T_w	wind return period
Hs	significance wave height (m)	u_i	uniform random number
H_{max}	maximum height of water (m)	V	wind speed over the surface of water (km/h)
H_R	height of dam (m)	V_{Tw}	wind speed in a specific return period (km/h)
Y_s	wind set up (m)	x_k	random variates
Y_r	wave run-up (m)	z	performance function
H_w	total weight height (m)	Z_f	flood performance function
I	inflow (m^3/s)	Z_fw	flood and wind performance function
km	kilometer	Δt	time interval (s)
L	load	a	risk
m	meter	ρ	density of water (kg/m^3)
MCM	million cubic meters	β	reliability index indicator
M_f	depth integrated wave moment flux per unit width	μ	mean of variable
$P[.]$	probability of.	σ	standard deviation
P_k	random permutation	θ	slope of the dam body

overtopping, which comprises about one third of all uncontrolled breach failures [1].

Traditionally, the approach to dam design focuses deterministic analysis on extreme events, such as probable maximum flood (PMF). PMF can be defined as amount of flood that may be expected from the most severe combination of meteorological and hydrologic conditions that are logically possible. In other words, PMF considers the upper range of flood potential and assumes zero-failure reliability. However, the standard dam design has not been absolutely solved because of the uncertainty in variables and applied models, and remains a difficult issue in hydrosystem engineering [2]. By improving the mathematical and statistical models, the increasing ability of computer programs, and the availability of data records for longer periods, it is time to move from the deterministic approaches in engineering design to probabilistic methods that consider higher order uncertainty in variables and models. Bowles [3] studied the tolerable risk concept in hydrosystem engineering and presented some examples for tolerable risk criteria in dam safety. Wang and Bowles [4] studied different breach locations of an earthen dam due to wave overtopping. Their results showed that wind direction, as well as wind speed, have an effect on breach location. Kwon and Moon [5] introduced three major innovations to improve overtopping risk elevations using probabilistic concepts for existing dams. The first comprises used nonparametric probability density estimation methods for selected variables; the second was applying Latin hypercube sampling to improve Monte Carlo simulation efficiency; and the third was the use of bootstrap re-sampling to determine initial water surface level. Marengo [6] studied the probability of overtopping during dam construction by focusing on upstream water surface elevation during flooding. Kuo et al. [7] conducted risk analysis for the Feitsui Reservoir by considering five uncertainty analysis methods (MFOSM, RPEM, HPEM, LHS, and MCS) and four initial water levels for five return periods. Goodarzi et al. [20] presented the application of risk and uncertainty analysis

to dam overtopping based on univariate and bivariate flood frequency analyses by applying Gumbel logistic distribution. Other researchers who investigated dam safety risk assessment were Wood [8], Cheng et al. [9,10], the Committee on the Safety of Existing Dams [11], and Singh and Snorrason [12,13].

This study presents a probability-based method for estimating dam overtopping probability by considering the uncertainty arising from peak discharges, initial water levels, and spillway discharge coefficient. The Monte-Carlo simulation (MCS) and Latin hypercube sampling (LHS), as the two most effective sampling approaches were applied to perform the uncertainty analysis. These results can be analyzed statistically to predict system behavior. As the accuracy of these methods strongly depends on sample size, large sample numbers (20,000 for Monte-Carlo and 10,000 for LHS) were considered in this study to increase calculation precision.

The overall process of risk and uncertainty analysis in this study includes the following steps: data collection, flood and wind frequency analysis, identification of uncertainty factors in the overtopping analysis, reservoir routing, and risk and uncertainty analyses (Fig. 1).

2. Dam risk model

If a system is unable to perform expected tasks, the system will fail, and, accordingly, undesirable consequences will occur. Failure can be defined as the load (L) exceeding system resistance or capacity (R). Identifying load and resistance is a fundamental issue in risk analysis and it noticeably depends on the type of hydraulic structure and problem physics. Tung et al. [14] defined the probability of failure as:

$$\text{Probability of failure} = P(L > R) \tag{1}$$

where $P[.]$ is the probability of failure.

Risk can also be represented as [16]:
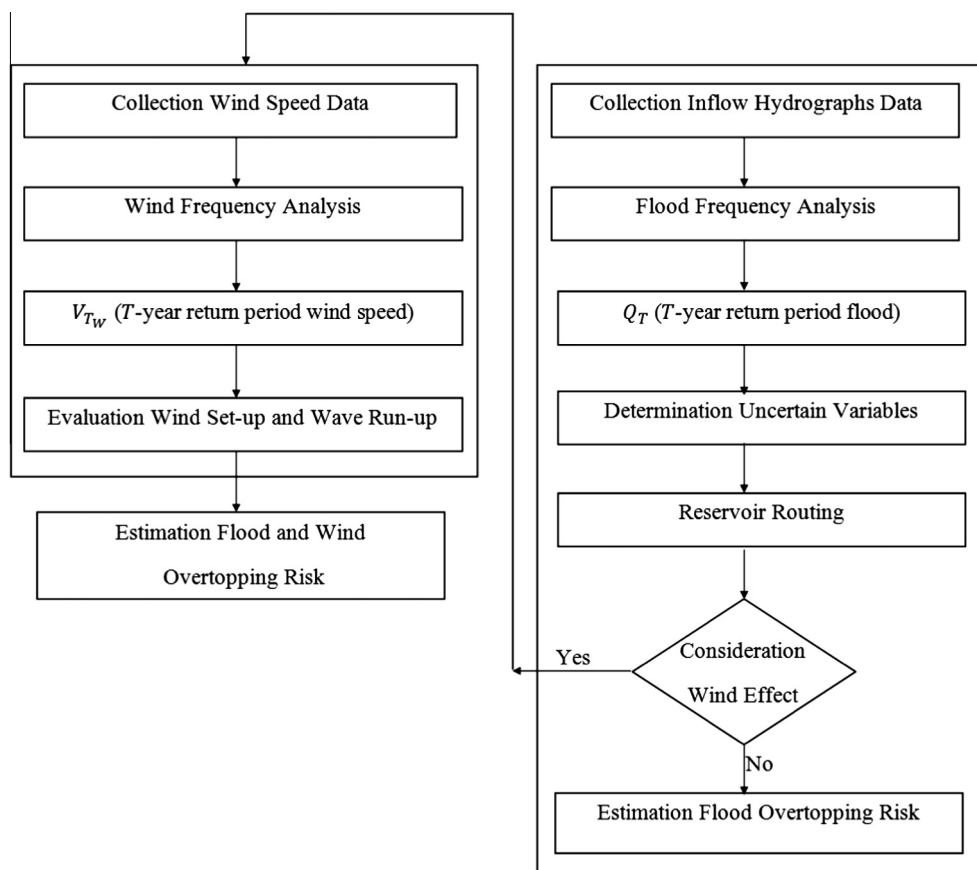
$$\alpha = \text{Risk} = P(Z < 0) \tag{2}$$

Figure 1 Flow chart for dam overtopping probability.

Table 1 Goodness-of-fit tests for the system outcomes.

T-Year	Goodness-of-fit test	Kolmogorov–Smirnov		Anderson–Darling	
	Probability distribution	Statistic value	Table value	Statistic value	Table value
2	Log-normal	0.009	0.030	0.183	2.501
2	Normal	0.015	0.030	0.818	2.501
10	Log-normal	0.009	0.030	0.183	2.501
10	Normal	0.015	0.030	0.818	2.501
20	Log-normal	0.011	0.030	0.209	2.501
20	Normal	0.018	0.030	0.886	2.501
50	Log-normal	0.011	0.030	0.214	2.501
50	Normal	0.018	0.030	0.899	2.501
100	Log-normal	0.011	0.030	0.208	2.501
100	Normal	0.018	0.030	0.884	2.501

where Z is performance function which can be defined as $Z = R - L$, $Z = (R/L) - 1$, and $Z = \ln(R/L)$.

The performance function of an engineering system can be described in several forms in which the selection of each form depends on the distribution type of the performance function. In this study, the system outcomes have been compared with the log-normal and normal distributions, and the goodness-of-fit test was applied to choose the appropriate distribution based on the Kolmogorov–Smirnov and Anderson–Darling tests (Table 1). The results of the test revealed that log-normal distribution fits the data better than normal distribution; and thus, the log form of performance function was selected. Hence, the form of performance function (Z) can be written as follows:

$$Z = \ln\left(\frac{R}{L}\right) \tag{3}$$

More information on various performance function forms and their application to hydraulic engineering systems are presented by Yen [15].

2.1. Risk modeling for flood and wind overtopping

Overtopping happens when the flood outlet cannot release water fast enough and water rises above the dam and spills over (Fig. 2). In overtopping analysis, the maximum water height in the reservoir (H_{max}) and dam height (H_R) can be
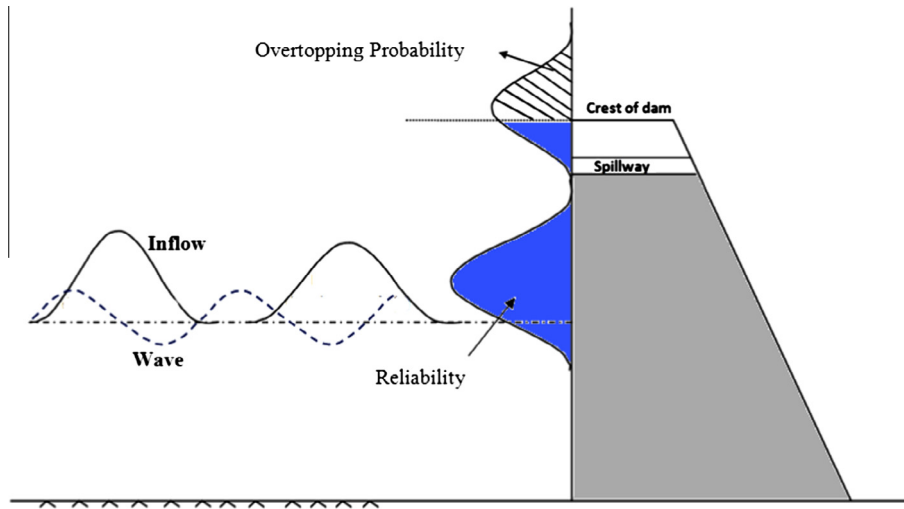
Figure 2 Overtopping risk concept based on probabilistic approach.

considered as the load and resistance of the system, respectively. Therefore, the overtopping probability with respect to the performance function due to different inflows and wind speeds can be expressed as follows [16]:

$$Z_f = \ln\left(\frac{H_R}{H_{max}}\right) \tag{4}$$

and

$$Z_{fw} = \ln\left(\frac{H_R}{H_{max} + H_w}\right) \tag{5}$$

where Z_f is flood performance function, Z_{fw} is flood and wind performance function, H_R is dam crest height, H_w is the total wave height, and H_{max} is the highest water level during a flood event, calculated based on reservoir routing. Finally, the overtopping probability will be computed as:

$$\text{Risk} = 1 - \emptyset\left(\frac{\mu_z}{\sigma_z}\right) = 1 - \emptyset(\beta) \tag{6}$$

in which β is the reliability index indicator and is defined as the mean ratio of the performance function (μ_z) to its standard deviation (σ_z).

3. Reservoir routing

The main objective of overtopping analysis of an earth-filled dam is estimating the water height in the reservoir under various inflows and wind speeds, and comparing the result with the dam crest elevation. The known, frequently used flood model, is the continuity equation with the following basic form:

$$I - Q = \frac{ds}{dt} \tag{7}$$

where I and Q are reservoir inflow and outflow (m³/s), s is storage (m³), and t is time (s). The implementation form of reservoir routing can be written as:

$$\frac{I_t + I_{t+1}}{2} - \frac{Q_t + Q_{t+1}}{2} = \frac{S_{t+1} - S_t}{\Delta t} \tag{8}$$

where I_t and I_{t+1} are inflow into the reservoir (m³/s), Q_t and Q_{t+1} are outflow from the reservoir (m³/s), S_t and S_{t+1} are reservoir storage (m³) at t and $t + 1$, respectively, and Δt is time interval (s).

The maximum water height in the reservoir could be estimated by solving Eq. (8) step by step. Time interval Δt determines the length of each step in the reservoir routing and output precision will be increased with decreasing Δt. In this study, a time interval of 30 min was selected to reduce uncertainty due to the highest water level possibility, which may occur between t and $t + 1$. The fourth order Runge–Kutta was applied to solve reservoir routing throughout this investigation.

4. Wind model

Wind can be defined as the horizontal movement of air, which is created if the thermal temperature balance changes because of unequal energy. Wind can start waves, raise the height of water in a reservoir, and, consequently, increase the probability of the occurrence of overtopping. In other words, if the water elevation is very near the crest, the generated waves might wash over and result in dam failure. Wind set-up and wave run-up are applicable factors in evaluating the effect of wind speed on the water surface elevation in reservoirs. Hence, there is a requirement to make a relationship between the wind return period (T_w) and wind speed in the desired return period (V_{Tw}) to calculate wind set-up, wave run-up, and the total height of water elevation. USBR [18,19] provided a method to estimate wind-generated waves in reservoirs, which is commonly accepted in the dam engineering community. Based on USBR [19], the minimum duration to reach a maximum wave height, t_{min} in hours, is calculated by the following equation:

$$t_{min} = 1.544 \frac{F^{0.66}}{V^{0.41}} \tag{9}$$

where V is the wind speed over water in km/h, and F is fetch length in km. The significant wave height H_s (m), which is the average of the highest one-third of the waves of a given

group or spectrum can be calculated by the following equation [19]:

$$H_s = 0.00237 V^{1.23} F^{0.5} \tag{10}$$

When wind hits the beach, a setup is created and the water level rises higher than the normal water level in the reservoir. This event is called wind set-up. USBR [19] has provided the following equation to compute wind set-up:

$$Y_s = \frac{V^2 F}{62772 D} \tag{11}$$

where Y_s (m) is wind set-up, F is fetch length km, V is wind speed over the water surface (km/h) and D (m) is mean water depth along the fetch length.

If a wave approaches or hits a structure, such as a dam, part of the energy is destroyed because of turbulence and the rest of the energy is used to run-up the dam embankment. Therefore, wave run-up is defined as the vertical difference between the highest water level caused by the run-up on the dam and the water level at the slope foot. According to the height of the run-up, it can be determined whether overtopping occurs or not. This parameter is a function of the measured wave characteristics including significant wave height, wavelength, slope of dam body roughness, and dam permeability. Hughes [17] presented an equation to compute the maximum wave run-up based on the wave moment flux as follows:

$$\frac{Y_R}{H_0} = 3.84 \cdot Tan\theta \cdot \left(\frac{M_F}{\rho \cdot g \cdot H_0^2} \right)^{1/2} \tag{12}$$

where Y_R is the maximum run-up of regular waves (m), H_0 is water depth from the bed to the current water elevation (m), M_f is depth integrated wave moment flux per unit width, ρ is the density of water (kg/m^3), and θ is the embankment slope. Hughes [17] also presented an empirical relationship for estimating momentum flux as follows:

$$\left(\frac{M_F}{\rho \cdot g \cdot H_0^2} \right)_{max} = A_0 \left(\frac{H_0}{gT^2} \right)^{-A_1} \tag{13}$$

where $A_0 = 0.6392(H/H_0)^{2.0256}$, $A_1 = 0.1804(H/H_0)^{-0.391}$, and H (m) is wave height, which can equal significant weight height [4]. Finally, the total wave height, which is an integration of the wind set-up and wave run-up in the reservoir, was calculated as follows:

$$H_w = Y_R + Y_S \tag{14}$$

5. Uncertainty analysis

In water resource engineering, making a decision about system operation and capacity is strongly dependent on the system's reaction under some predictable conditions. However, it is not possible to assess the system's reaction with distinct certainty, as the various system components are subject to different kinds of uncertainty. Uncertainty refers to the condition or variable, which is not able to be quantified exactly and it has random characteristics. One problem regarding the different uncertain variables in complex and non-linear models like reservoir routing is deriving the PDF of uncertain variables and determining the appropriate statistical moments or probability distribution of model outputs. Furthermore, any analysis in the real world is based on historical recorded data, while usually historical records are not long enough and the data includes all sorts of errors. Sampling is potentially an applicable method to compound several random input values and get results with appropriate accuracy. Hence, the Monte Carlo simulation and Latin hypercube sampling, as two significant sampling techniques, were used in this study to quantify the uncertainty in overtopping analysis.

5.1. Monte Carlo simulation (MCS)

Simulation is a process of recreating a real situation, usually based on a set of hypotheses and mathematical formula. Simulation is a useful tool for evaluating system performance in different conditions and also to test new theories in the form of a computer program. The Monte Carlo process is a numerical simulation that replicates stochastic variables according to a certain statistical distribution. In other words, Monte Carlo uses random numbers to model a desired process. To generate continuous random numbers based on the Monte Carlo simulation, consider X as a random variable and $F_x(X)$ as its cumulative distribution function (CDF), the inverse function for any value of $u \sim u(0, 1)$ can be written as:

$$X = F_x^{-1}(u) \tag{15}$$

where $F_x^{-1}(u)$ is the inverse function and u has a uniform distribution on (0, 1).

It should be noted that the continuous probability distributions in hydrosystem engineering is strictly uptrend for all random variables X and thus, there is a unique relationship between $F_x(x)$ and u as $u = F_x(X)$. To generate m random variables using the CDF-inverse method, the following steps should be repeated m times:

1. Draw a uniform random variate as $u \sim u(0, 1)$, (random number generator).
2. Find x such that $x = F_x^{-1}(u)$.

There are two major concerns about the Monte Carlo simulation. First, it needs large computations to generate random values, and second, result accuracy strongly depends on the number of iterations and simulations. In the Monte Carlo simulation increasing sample size is a pre-requisite to achieving higher precision results. However, the achieved results will lead to sampling errors related to the number of selected random variates with an inverse relation to the sample size number. On the other hand, increasing sample size entails an increase in computer time needed for generating random variates and the simulation process.

5.2. Latin hypercube sampling (LHS)

There are some reduction variance techniques to increase the precision of the Monte Carlo simulation outcome without needing to increase the sample size [14]. Some of the most important methods of variance reduction are antithetic-variates technique, control variates, importance sampling technique, Latin hypercube sampling (LHS), correlated sampling, and stratified sampling technique [14]. LHS is one of the main variance reduction techniques that can increase the efficiency of the output statistics parameters. In this method, the range of each variable is divided into n non-overlapping intervals
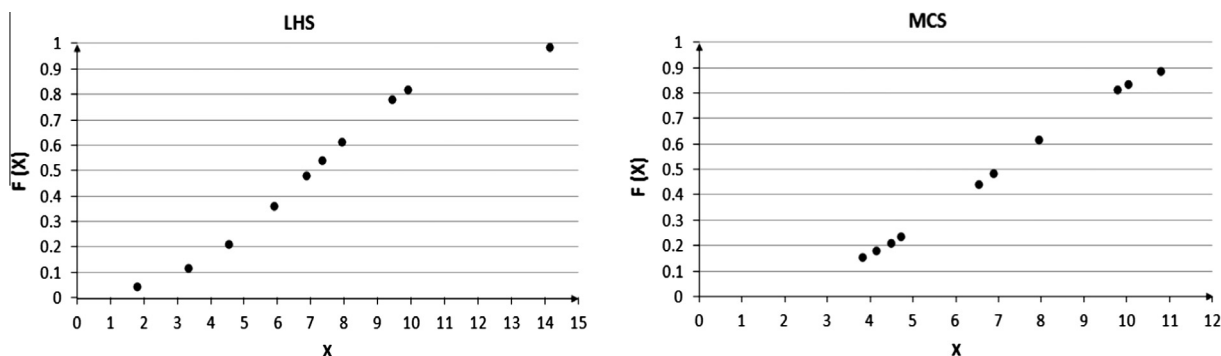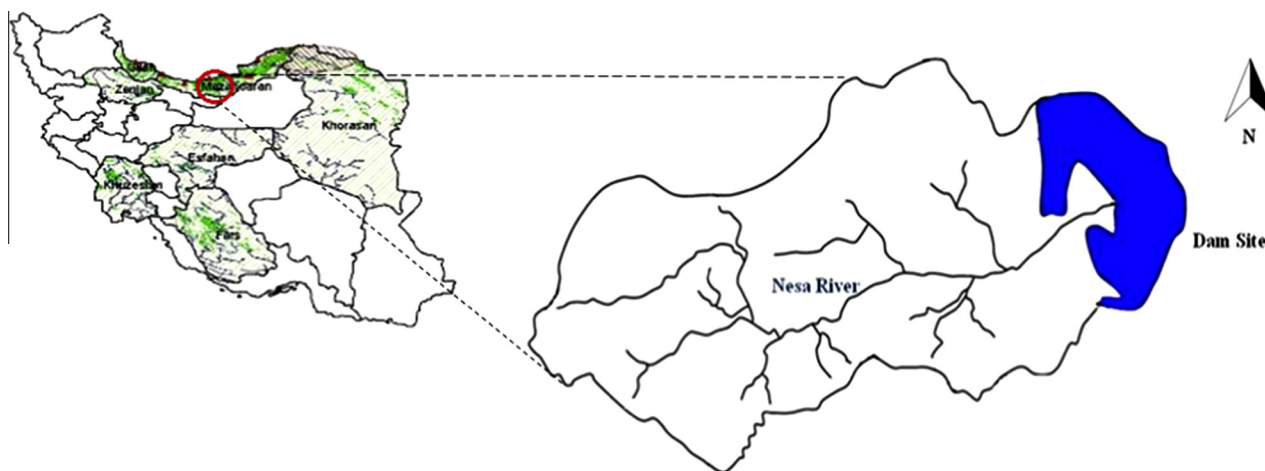
Figure 3   Comparison of LHS and MCS outcomes.

Figure 4   The schematic view of Meijaran basin.

Table 2   Goodness of fit test of the maximum annual flood.

Probability distribution	Anderson–darling		
	Statistic value	Table value	Remark
Gumbel Max	0.274	2.501	Ok
GEV[a]	0.201	2.501	Ok
Log–Logistic	0.270	2.501	Ok
Gamma	0.226	2.501	Ok
Log-Gamma	0.363	2.501	Ok
Pearson 5 (3P)	0.243	2.501	Ok
Log-Pearson 3	0.207	2.501	Ok
Normal	0.742	2.501	Ok

[a] General extreme value.

with the equal probability $1/n$. Then, a random variate is selected from each range with regards to the desire probability distribution [16]. A simple and primary algorithm for applying the LHS method is:

1. Determine n.
2. Generate random uniform variates $u_K \sim u(0, 1)$.
3. Calculate P_k from the following equation:

$$P_k = \frac{1}{n} u_k + \left(\frac{k-1}{n} \right) \qquad (16)$$

where $k = 1, 2, \ldots, n$.

4. Determine random variates x_k from the inverted CDF as follows [5]:

$$X_k = F^{-1}[P_k] \qquad (17)$$

The main difference between LHS and MCS outcomes is shown in Fig. 3, where each generated random variate from the LHS is placed in a separate interval with the equal probability $1/n$. In other words, each region only includes one random variate, while the generated random variates from the Monte Carlo (MC) technique are randomly distributed and there may be more than one random variate, or no random variate placed in an equal probability area.

6. Overtopping probability of existing dam

6.1. Study area and data collection

The proposed hydrologic dam risk was applied to the Meijaran Dam in the north of Iran. The dam basin is located near the south-west of the Caspian Sea, on the Nesa River. The Nesa River watershed is between 50°35′ and 50°42′ longitude 36°49′ and 36°52′ latitude. The elevation of the watershed's highest point is 2143 m above the mean sea level with the average slope of 39% at the mountains part. The schematic view of the Meijaran Basin is shown in Fig. 4.

Table 3 Mean and standard deviation of inflows to Meijaran Reservoir.

T-Year	2-Years	10-Years	20-Years	50-Years	100-Years
μ_1	9.54	41.82	56.16	77.68	84.674
σ_1	1.10	6.74	12.03	22.92	31.13

μ_1: Mean of peak discharges and σ_1: standard deviation of peak discharges.

Table 4 Goodness of fit test for maximum annual wind speed.

Probability distribution	Anderson–darling		
	Statistic value	Table value	Remark
Gumbel Max	0.842	2.501	Ok
GEV[a]	0.806	2.501	Ok
Weibull	1.228	2.501	Ok
Gamma	0.832	2.501	Ok
Normal	0.941	2.501	Ok
Log-Normal (3P)	0.810	2.501	Ok
Pearson 5 (3P)	0.804	2.501	Ok
Log-Pearson 3	0.795	2.501	Ok
Log-Gamma	0.811	2.501	Ok
Gamma (3P)	0.832	2.501	Ok

[a] General extreme value.

The construction of Meijaran Dam with a 186 m crest length and 55 m height was started in 1996 and was completed in 2003. The most important objectives for building this dam were to supply agricultural water for 2050 ha, especially tea farms, flood prevention along the Nesa River, secure domestic supplies to downstream cities, and tourism development. All daily inflow data (1968–2008) into the reservoir and daily reservoir water elevation (2003–2009) were collected by the Mazandaran Ministry of Energy Data Center land based/surface data collection. Team members collected all available daily meteorological data including inflows, water elevation, rainfall, temperature, etc., for each station along the Nesa River, and the recorded data were imported in Microsoft Excel workbooks for data quality assurance/quality control. The four continuous-record stream flow gaging stations on the Nesa River are (1) Ramsar station, (2) ChalakRud station, (3) Tir or Shirrud station, and (4) Haratbar station.

6.2. Flood frequency analysis

Different statistical distributions were fitted to the annual maximum floods in order to estimate the peak flows in various return periods. The used distributions were: Gumbel Max,

General Extreme Value (GEV), Gamma, Log-Gamma, Log–Logistic, Normal, Pearson 5 (3P), and Log-Pearson 3. Afterward, a goodness-of-fit test was applied to choose the appropriate distribution based on the Anderson–Darling test (Table 2). Although the result of test demonstrated that all distributions considered could be selected for recorded flood data, the GEV distribution fits better than other distribution. From frequency analysis, the values of mean and standard deviation of estimated peak discharge were obtained at a given return period and the results are presented in Table 3.

6.3. Wind flood frequency analysis

According to recorded monthly wind data for 33 years, there are two main wind speed directions in the Meijaran Dam basin, namely, north-west and west. Although the west wind
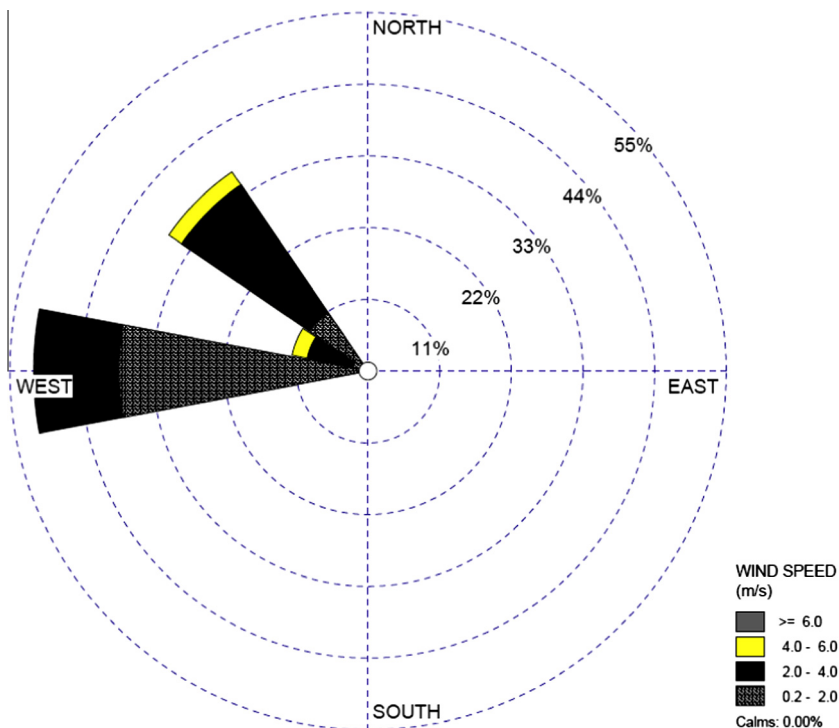

Figure 5 Wind rose of Meijaran basin.

Table 5 Value of wind speed and minimum duration to reach maximum wave height.

T-Year	CDF	V (km/h)	t_{min} (h)
2	0.500	15.73	0.164
10	0.900	23.64	0.139
20	0.950	26.82	0.132
50	0.980	31.09	0.124
100	0.990	34.42	0.119

T: Return period, CDF: cumulative density function, V: wind speed, and t_{min}: minimum duration of wind.

Table 6 Statistical properties for uncertain parameters.

Variable	Type	PDF	μ	σ
H_0	Random	Normal	46.0	1.01
I	Random	GEV	Table 2	Table 2
c	Random	Normal	2.13	0.071

H_0: Initial water depth, I: inflow discharge, c: discharge coefficient, μ: mean, and σ: standard deviation.

speed is less than the north-west wind speed, the direction of the west wind is along the fetch length and can generate higher waves. The wind rose of Meijaran basin is presented in Fig. 5.

In this regard, the west wind data is applied to evaluate the wind set-up and wave run-up in Meijaran's reservoir. Different statistical distributions were fitted to the 33 years (1975–2008) annual maximum wind speed in order to estimate the maximum speeds in various return periods. The distributions utilized were: Gumbel max, General extreme value, Gamma, Log-gamma, Gamma 3P, Weibull, Log-normal 3P, Normal, Pearson 5 (3P), and Log-Pearson 3. A goodness-of-fit test was applied to select the appropriate distribution based on the Anderson–Darling test and the results showed the

Log-Pearson III distribution fits better than other distribution, and, thus, it was selected for frequency analysis of wind speed data (Table 4). Afterwards, the values of wind speeds were computed at 2, 10, 20, 50, and 100-year return periods and the results are presented in Table 5.

6.4. Uncertainty analysis

The considered uncertainty parameters in this study are as follows:

1. Quantile of flood peak discharge in different return periods (I): the main reasons for considering peak floods as uncertain variables are error in data recording, lack of data, and lateral inflow into the reservoir. The values of mean and standard deviation of peak discharges for the Meijaran Reservoir are presented in Table 3. The estimated peak discharges based on GEV distribution have been used to generate inflow hydrographs, and then, the generated hydrographs were routed into the reservoir to compute the maximum water height.

2. The initial water level (H_0): the average depth of water in the reservoir was computed based on the observed and recorded water elevation over 6 years (2003–2009) during the wet seasons. The mean and standard deviation of water depth were 46.0 (m) and 1.01 (m), respectively. In addition, six more depths (at 1.5 m increments) were assumed as initial water depth to consider the effect of changing initial water depth on the probability of overtopping.

3. Spillway discharge coefficient (C): its mean and standard deviation were assumed to be 2.13 and 0.071, respectively.

The specifications of input parameters, such as mean μ standard deviation (σ), and the probability distribution function (PDF), which were fitted to the random uncertain data, are presented in Table 6.

Table 7 Risk of overtopping by Monte Carlo method due to different floods.

H_0 (m)	T				
	2-Year	10-Year	20-Year	50-Year	100-Year
46.0	1.97E−12	3.41E−11	2.94E−10	6.34E−09	9.91E−08
47.5	6.29E−11	5.96E−10	3.37E−09	4.60E−08	4.75E−07
49.0	6.09E−10	1.63E−08	1.14E−07	5.60E−07	5.64E−06
50.5	5.20E−08	5.94E−07	4.03E−06	1.17E−05	2.12E−05
52.0	3.91E−07	2.91E−06	1.64E−05	4.66E−05	9.23E−05

H_0: Initial water depth and T: flood return period.

Table 8 Risk of overtopping by LHS method due to different floods.

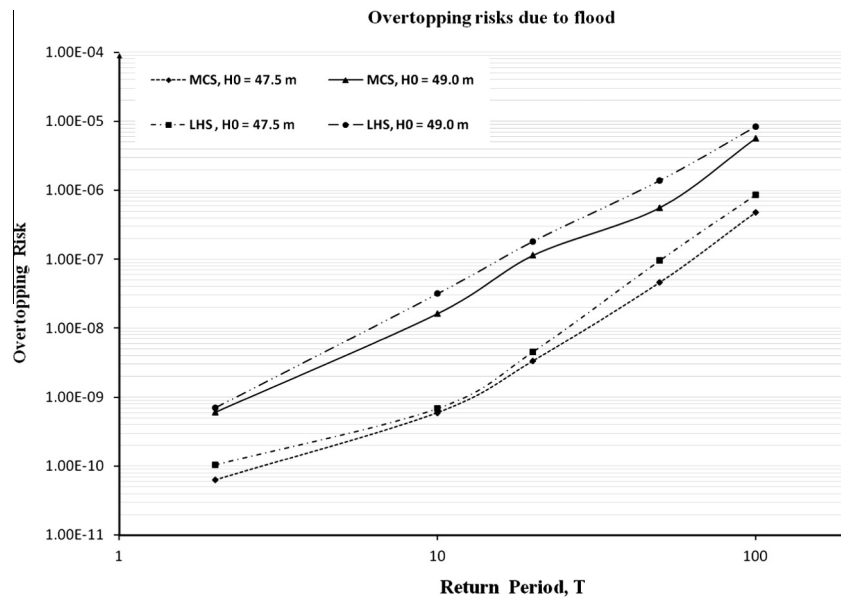| H_0 (m)	T				
	2-Year	10-Year	20-Year	50-Year	100-Year
46.0	9.84E−12	9.30E−11	5.28E−10	7.51E−09	1.51E−07
47.5	1.04E−10	6.86E−10	4.57E−09	9.64E−08	8.64E−07
49.0	7.09E−10	3.16E−08	1.82E−07	1.38E−06	8.29E−06
50.5	1.37E−07	1.22E−06	6.63E−06	2.49E−05	5.90E−05
52.0	9.65E−07	7.55E−06	2.84E−05	1.12E−04	1.72E−04

Figure 6 Flood overtopping risks at initial water level 47.5 and 49.0 m based on MCS and LHS methods.

6.5. Overtopping probability due to different floods

Based on the equations presented in the previous sections, the probability of overtopping was calculated for various floods at 2, 10, 20, 50, and 100-year return periods by con-sidering three uncertain variables as peak discharge, initial water level, and spillway discharge coefficient. All uncertain variables were assumed to be independent variables, while the Monte-Carlo simulation (with a sample size of 20,000) and Latin hypercube sampling (with a sample size of

Table 9 Risk of Overtopping due to flood and wind using MCS.

T_w	H_0 (m)	T				
		2-Years	10-Years	20-Years	50-Years	100-Years
2-Years	46.0	2.27E−12	5.42E−11	4.61E−10	1.10E−08	2.00E−07
	47.5	7.27E−11	9.48E−10	5.26E−09	7.95E−08	9.52E−07
	49.0	7.03E−10	2.60E−08	1.78E−07	9.61E−07	1.12E−05
	50.5	6.00E−08	9.43E−07	6.25E−06	2.00E−05	4.18E−05
	52.0	4.55E−07	4.66E−06	2.63E−05	8.44E−05	9.76E−05
10-Years	46.0	4.12E−12	9.47E−11	7.41E−10	2.59E−08	4.09E−07
	47.5	1.32E−10	1.65E−09	8.42E−09	1.85E−07	9.73E−07
	49.0	1.27E−09	4.53E−08	2.83E−07	2.22E−06	5.60E−05
	50.5	1.08E−07	1.64E−06	9.92E−06	4.59E−05	8.34E−05
	52.0	8.30E−07	8.20E−06	4.33E−05	2.06E−04	4.15E−04
20-Years	46.0	8.12E−12	1.35E−10	1.19E−09	6.07E−08	8.35E−07
	47.5	2.59E−10	2.88E−09	1.35E−08	4.31E−07	1.97E−06
	49.0	2.50E−09	7.89E−08	4.51E−07	5.14E−06	1.16E−05
	50.5	2.13E−07	2.86E−06	1.57E−05	1.06E−04	5.55E−04
	52.0	1.65E−06	1.44E−05	7.13E−05	5.02E−04	8.86E−04
50-Years	46.0	1.60E−11	1.93E−10	1.91E−09	1.42E−07	1.70E−06
	47.5	5.11E−10	4.12E−09	3.28E−08	8.79E−07	3.99E−06
	49.0	4.93E−09	1.12E−07	7.19E−07	9.53E−06	4.08E−05
	50.5	4.20E−07	4.07E−06	2.50E−05	4.52E−04	9.97E−04
	52.0	3.29E−06	2.08E−05	1.17E−04	9.22E−04	1.89E−03
100-Years	46.0	3.16E−11	4.91E−10	3.07E−09	3.33E−07	3.48E−06
	47.5	1.01E−09	1.05E−08	5.25E−08	2.05E−06	8.08E−06
	49.0	9.71E−09	2.85E−07	1.15E−06	2.20E−05	8.19E−05
	50.5	8.25E−07	1.03E−05	5.91E−05	1.04E−03	5.93E−03
	52.0	6.54E−06	5.31E−05	3.35E−04	2.25E−03	9.05E−03

T_w: Wind speed return period, T: flood return period, and H_0: initial water level.

Table 10 Risk of Overtopping due to flood and wind using LHS.

T_w	H_0 (m)	T				
		2-Years	10-Years	20-Years	50-Years	100-Years
2-Years	46.0	1.14E−11	1.48E−10	8.28E−10	1.31E−08	3.05E−07
	47.5	1.20E−10	1.09E−09	7.15E−09	1.67E−07	1.73E−06
	49.0	8.18E−10	5.03E−08	2.83E−07	2.37E−06	1.65E−05
	50.5	1.59E−07	1.94E−06	1.03E−05	4.25E−05	1.17E−04
	52.0	1.12E−06	1.21E−05	4.57E−05	2.02E−04	3.63E−04
10-Years	46.0	2.06E−11	2.59E−10	1.33E−09	3.07E−08	6.22E−07
	47.5	2.17E−10	1.90E−09	1.14E−08	3.88E−07	1.77E−06
	49.0	1.48E−09	8.77E−08	4.51E−07	5.49E−06	4.96E−05
	50.5	2.87E−07	3.38E−06	1.63E−05	9.76E−05	2.33E−04
	52.0	2.05E−06	2.13E−05	7.52E−05	4.93E−04	1.54E−03
20-Years	46.0	4.07E−11	3.69E−10	2.14E−09	7.19E−08	1.27E−06
	47.5	4.29E−10	3.32E−09	1.83E−08	9.03E−07	3.58E−06
	49.0	2.92E−09	1.53E−07	7.18E−07	1.27E−05	9.96E−05
	50.5	5.64E−07	5.88E−06	2.59E−05	2.24E−04	1.55E−03
	52.0	4.07E−06	3.74E−05	1.24E−04	1.20E−03	3.30E−03
50-Years	46.0	8.02E−11	5.27E−10	3.43E−09	1.69E−07	2.59E−06
	47.5	8.44E−10	4.74E−09	4.46E−08	1.84E−06	7.26E−06
	49.0	5.74E−09	2.18E−07	1.14E−06	2.35E−05	3.49E−04
	50.5	1.11E−06	8.37E−06	4.11E−05	9.62E−04	2.78E−03
	52.0	8.11E−06	5.39E−05	2.04E−04	2.21E−03	7.04E−03
100-Years	46.0	1.58E−10	1.34E−09	5.52E−09	3.95E−07	5.29E−06
	47.5	1.66E−09	1.20E−08	7.14E−08	4.29E−06	1.47E−05
	49.0	1.13E−08	5.53E−07	1.82E−06	5.44E−05	7.01E−04
	50.5	2.18E−06	2.12E−05	9.71E−05	2.21E−03	1.65E−02
	52.0	1.61E−05	1.38E−04	5.80E−04	5.39E−03	3.37E−02

T_w: Wind speed return period, T: flood return period; and H_0 = initial water level.
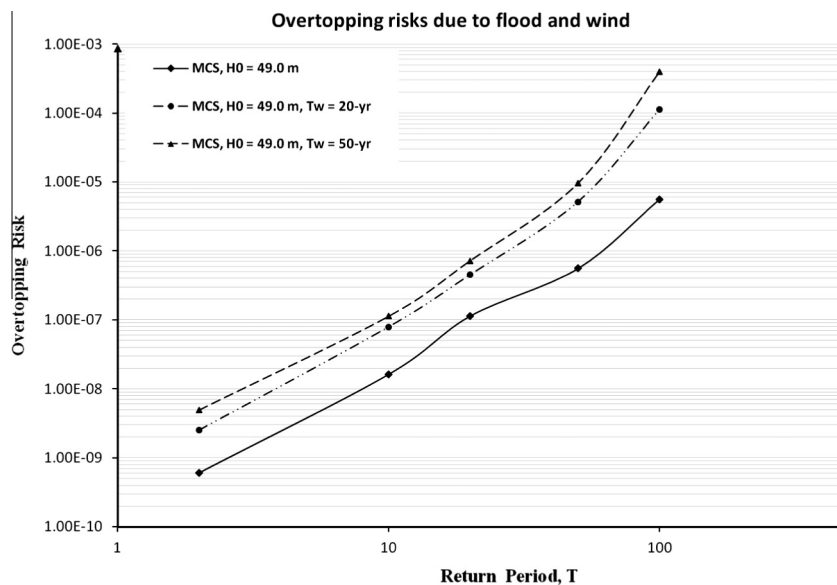

Figure 7 Overtopping risk versus different return periods with and without considering wind speeds, in the initial water level $H_0 = 49.0$ m.

10,000) were applied for uncertainty analysis. The probability of overtopping due to floods in different return periods and initial water levels for both MCS and LHS methods are presented in Tables 7 and 8. Based on the results, by increasing the initial water level in each step, the probability of overtopping (in a constant return period) was raised for both uncertainty approaches adopted in this study. Fig. 6 shows the variation of overtopping probability for the initial water levels of 47.5 (m), and 49.0 (m) in both the MCS and LHS methods.
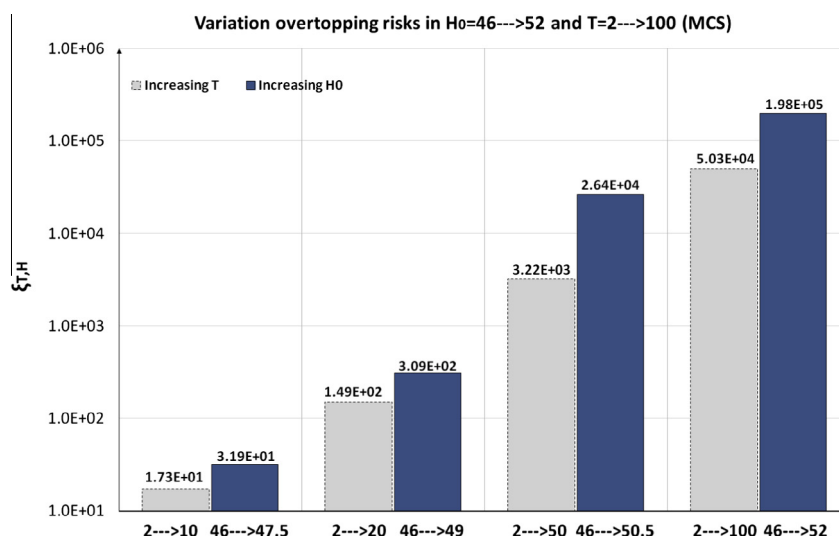
Figure 8 Variation overtopping risks by increasing return periods and water level (MCS).

Table 11 Ratio of overtopping risks in different H_0 and T to risk in $H_0 = 46$ and $T = 2$ (MCS).

H_0	$\xi_{T,H}$				
T	$2\rightarrow2$	$2\rightarrow10$	$2\rightarrow20$	$2\rightarrow50$	$2\rightarrow100$
46–46.0	1.00E+00	1.73E+01	1.49E+02	3.22E+03	5.03E+04
46–47.5	3.19E+01	3.03E+02	1.71E+03	2.34E+04	2.41E+05
46–49.0	3.09E+02	8.27E+03	5.79E+04	2.84E+05	2.86E+06
46–50.5	2.64E+04	3.02E+05	2.05E+06	5.94E+06	1.08E+07
46–52.0	1.98E+05	1.48E+06	8.32E+06	2.37E+07	4.69E+07

Table 12 Ratio of overtopping risks in different H_0 and T to risk in $H_0 = 46$ and $T = 2$ (LHS).

H_0	$\xi_{T,H}$				
T	2–2	2–10	2–20	2–50	2–100
46–46.0	1.00E+00	9.45E+00	5.37E+01	7.63E+02	1.53E+04
46–47.5	1.06E+01	6.97E+01	4.64E+02	9.80E+03	8.78E+04
46–49.0	7.21E+01	3.21E+03	1.85E+04	1.40E+05	8.42E+05
46–50.5	1.39E+04	1.24E+05	6.74E+05	2.53E+06	6.00E+06
46–52.0	9.81E+04	7.67E+05	2.89E+06	1.14E+07	1.75E+07

6.6. Overtopping probability due to flood and wind

The wind set-up and wave run-up were calculated using the equations provided by USBR [19]. It should be noted that there is no strong correlation between wind speed and inflows (*Corr* = 0.178), and, thus, the wind speeds and flood values were generated separately. In other words, the highest water level in the reservoir and total wave height were calculated individually, after that the total water elevation which is the sum of these two factors, was considered in the risk analysis. However, many combinations of inflows, wind speeds, and water elevation were considered to cover the most likely conditions that will probably happen in the reservoir. The overtopping probabilities due to different floods and wind speeds in five return periods and five initial water levels were evaluated by MCS and LHS uncertainty approaches (Tables 9 and 10). According to the results, the overtopping probabilities increases by increasing the flood return period for both the Monte-Carlo and Latin hypercube techniques. The risk of overtopping, based on the MCS method versus different return periods with and without considering wind speeds at the initial water level $H_0 = 49.0$ m, is shown in Fig. 7.

To show how the risks of overtopping changed with increasing water levels and return periods, and also to compare the achieved results, ratio $\xi_{T,H}$ was defined as:

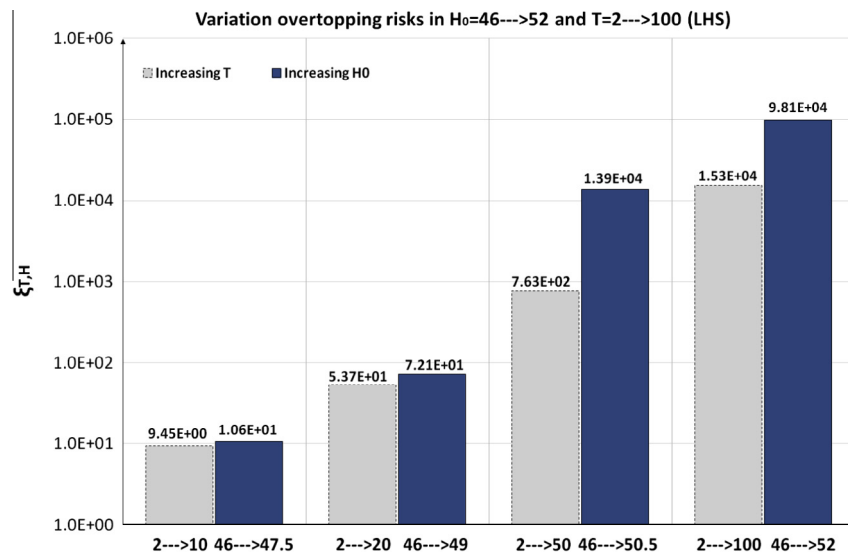$$\xi_{T,H} = \frac{\text{Risk}_{T,H}}{\text{Risk}_{T=2,H_0=46}} \qquad (18)$$

Figure 9 Variation overtopping risks by increasing return periods and water level (LHS).

where $\text{Risk}_{T,H}$ is the overtopping probability in a particular return period and water level, and $\text{Risk}_{T=2,H_0=46}$ is the overtopping probability in $T = 2$ and $H_0 = 46$.

The results demonstrated that rising water levels greatly impact the probability of overtopping compared with the return periods in both MCS and LHS methods (Table 11 and 12). Furthermore, the ratio of overtopping probabilities in $H_0 = 46{-}52$ and $T = 2{-}10$ for both MCS and LHS methods are presented in Figs. 8 and 9.

It should be noted that LHS stratifies the cumulative density function (CDF) into several sub-regions while the generated random variates from the Monte Carlo (MC) technique are randomly distributed. Hence, the achieved outcomes from adopted uncertainty approaches are not similar in this study.

7. Conclusions

Risk and uncertainty analysis can be employed to evaluate the probability of dam failure regarding overtopping, internal erosion, geological instability, and earthquakes. This paper demonstrated the process of estimating overtopping probability due to various inflows and wind speeds for Meijaran Dam in the north of Iran. The procedure included flood and wind speed frequency analysis, reservoir routing, and integration of wind set-up and run-up to calculate the final reservoir water level. The probability of overtopping was assessed by applying two uncertainty analysis methods (MCS and LHS) and considering the quantile of flood peak discharge, initial depth of water in the reservoir, and spillway discharge coefficient as uncertain variables.

From these results it can be concluded that rising water levels in the reservoir would result in the increasing overtopping probability based on both the MCS and LHS techniques. For instance, the probability of overtopping in $T = 20$-year from $H_0 = 46$ to $H_0 = 49$ increased from $5.28\text{E}{-}10$ to $1.82\text{E}{-}07$ based on the MCS and LHS methods, respectively. On the other hand, the results revealed that wind speed could have a great impact on reservoirs situated in windy areas. Dam overtopping probabilities at $T = 20$-year, $T = 2$-year and $H_0 = 49$ were found to be 56.14% and 55.49% greater than the risk in the same condition without considering the wind effect.

All in all, risk analysis provides an expanded range of risk values in different return periods such that the dam administrator can identify the events that indicate a developing failure mode, understand the critical parameters needed to effectively monitor, and determine how to use a warning system for evacuating the downstream community. Meanwhile, deterministic methods use only the best estimate inputs and provide a single point as output.

8. Future studies

In this study, only three variables were considered as uncertain factors, while other variables, such as precipitation, reservoir geometry, dam height, and time to peak of inflow hydrographs, can be assumed to be uncertain variables. In addition, all factors contributing to overtopping probability are assumed as independent variables, which can be a problem in real situations where these factors are dependent. Under these circumstances, bivariate or multivariate frequency analysis would be useful and could convey the dependence between variables.

References

[1] International Commission on Large Dams. Lessons from dam incidents (reduced edition). ICOLD, Paris; 1973.

[2] Stedinger JR, Heath DC, Thompson K. Risk analysis for dam safety evaluation: hydrologic risk. US Army Corps of Engineers Institute for Water Resources: Cornel University; 1996.

[3] Bowles DS. Evaluation and use of risk estimates in dam safety decision making. In: 20-Year retrospective and prospective of risk-based decision-making. Santa Barbara (California): ASCE; 2001. p. 17–32.

[4] Wang Z, Bowles DS. Dam breach simulations with multiple breach locations under wind and wave actions. Adv Water Resour 2005;29:1222–37.

[5] Kwon H, Moon Y. Improvement of overtopping risk evaluations using probabilistic concepts for existing dams. Springer; 2006.

[6] Marengo H. Case study: dam safety during construction, lessons of the overtopping diversion works at Aguamilpa Dam. J Hydraulic Eng 2006;132:1121–7.

[7] Kuo JT, Yen BC, Hsu YC, Lin HF. Risk analysis for dam overtopping – Feitsui Reservoir as a case study. J Hydraulic Eng 2008;133:955–63.

[8] Wood EF. An analysis of flood levee reliability. Water Resour Res 1977;13:665–71.

[9] Cheng ST, Yen BC, Tang WH. Overtopping risk for an existing dam. Civil engineering studies. Hydraulic Eng Ser 1982:37.

[10] Cheng ST, Yen BC, Tang WH. Wind-induced overtopping risk of dams. In: Yen BC, editor. Stochastic and risk analysis in hydraulic engineering. Littleton (CO): Water Resources Publications; 1986.

[11] Committee on the Safety of Existing Dams. Water science and technology board. commission on engineering and technical systems and national research council. Safety of existing dams' evaluation and improvement. Washington (DC): National Academy Press; 1983.

[12] Singh KP, Snorrason A. Sensitivity of outflow peaks and flood stages to the selection of dam breach parameters and simulation models. Technical report 289, USA: State Water Survey Division at the University of Illinois; 1982.

[13] Singh KP, Snorrason A. Sensitivity of outflow peaks and flood stages to the selection of dam breach parameters and simulation models. J Hydrol 1984;68:295–310.

[14] Tung YK, Yen BC, Melching CS. Hydrosystems engineering reliability assessment and risk analysis. New York: McGraw-Hill Professional; 2005.

[15] Yen BC. Safety factor in hydrologic and hydraulic engineering design. In: McBean EA, Hipel KW, Unny TE, editors. Reliability in water resources management. Highlands Ranch: Water Resources Publications; 1979.

[16] Singh VP, Jain SK, Tyagi A. Risk and reliability analysis. Am Soc Civ Eng 2007.

[17] Hughes SA. Estimation of wave run-up on smooth impermeable slopes using the wave momentum flux parameter. Coast Eng 2004;51:1085–104.

[18] USBR. Freeboard criteria and guidelines for computing freeboard allowances for storage dams. Denver (CO): US Dept of the Interior, Bureau of Reclamation; 1981.

[19] USBR. Freeboard criteria and guidelines for computing freeboard allowances for storage dams. Denver (CO): US Dept of the Interior, Bureau of Reclamation; 1992.

[20] Goodarzi E, Mirzaei M, Ziaei M. Evaluation of dam overtopping risk based on univariate and bivariate flood frequency analyses. Canad J Civ Eng 2012;39:374–87.